Flexural resonance vibrations of piezoelectric ceramic tubes in Besocke-style scanners*

Zhang Hui(张 辉)†, Zhang Shu-Yi(张淑仪), and Fan Li(范 理)

Laboratory of Modern Acoustics, Institute of Acoustics, Nanjing University, Nanjing 210093, *China*

(Received 2 December 2011; revised manuscript received 6 January 2012)

Flexural resonance vibrations of piezoelectric ceramic tubes in Besocke-style scanners with nanometer resolution are studied by using an electro-mechanical coupling Timoshenko beam model. Meanwhile, the effects of friction, the first moment, and moment of inertia induced by mass loads are considered. The predicted resonance frequencies of the ceramic tubes are sensitive to not only the mechanical parameters of the scanners, but also the friction acting on the attached shaking ball and corresponding bending moment on the tubes. The theoretical results are in excellent agreement with the related experimental measurements. This model and corresponding results are applicable for optimizing the structures and performances of the scanners.

Keywords: flexural resonance vibration, Timoshenko beam theory, Besocke-style scanner

PACS: 33.20.Tp, 43.40.+s, 46.55.+d, 07.79.Sp **DOI:** 10.1088/1674-1056/21/8/083302

1. Introduction

In manufacturing scanning probe microscopes (SPM), such as the scanning tunneling microscope (STM) and the atomic force microscope (AFM), an important technology is to provide the scanning systems with resolution on the nanometer scale and with high speed, accuracy, and load capacity.[1−3] Thus the Besocke-style scanner has become a popular configuration, owing to its advantages, such as simple structure, compact size, good thermal stability, and so on. Many Besocke-style scanners with high performances have been designed.[4−6]

In practical cases, SPMs are always affected by ambient noise, and the weak mechanical noise may severely affect the results. To improve the signal-to-noise ratio, the Besocke-style scanner should be designed with a much higher resonance frequency. Furthermore, the high resonance frequency can also increase scanning speed.[7] Therefore, there have been many studies on the resonance vibrations of the piezoelectric ceramic tubes of Besocke-style scanners. For example, by studying the eigenfrequencies of the flexural modes of the piezoelectric ceramic tube, the fundamental flexural resonance frequencies of the scanner can be given, in which the piezoelectric ceramic tube is regarded as a massless tube.[6] In addition, the Euler beam theory combined with Rayleigh's quotient has been used to calculate the resonance frequencies, in which three kinds of vibrational modes were analysed.[6−9] However, for short and thick piezoelectric ceramic tubes, there are large errors in theoretical investigations. For several practical scanners with resolution on the nanometer scale, the existing models cannot reveal how the friction acting on the attached ball and corresponding bending moment affect the flexural vibration of the piezoelectric ceramic tubes.[10]

In the present paper, a physical theory based on the Timoshenko beam model with exact boundary conditions is presented to investigate flexural vibration of a piezoelectric ceramic tube as a saw-tooth like voltage is applied to the tube, in which the main factors, such as the effects of shear deformation, rotary inertia, friction, and piezoelectricity of the piezoelectric ceramic tubes, etc. are considered.

2. Timoshenko beam model with the effect of piezoelectricity

For Besocke-style scanners, according to the Timoshenko beam model, the dynamic equations of the

*Project supported by the National Basic Research Program of China (Grant No. 2012CB921504), the National Natural Science Foundation of China (Grant Nos. 11004099 and 11174142), the State Key Laboratory of Acoustics of the Chinese Academy of Sciences, and the Priority Academic Program Development of Jiangsu Higher Education Institutions.

†Corresponding author. E-mail: paslabw@nju.edu.cn

© 2012 Chinese Physical Society and IOP Publishing Ltd

piezoelectric ceramic tube can be expressed as

$$\begin{cases} \rho A \dfrac{\partial^2 w}{\partial t^2} - \dfrac{\partial Q}{\partial z} = 0, \\ Q - \dfrac{\partial M}{\partial z} - \rho I \dfrac{\partial^2 \psi}{\partial t^2} = 0, \end{cases} \tag{1}$$

where ρ is the density, A the area of cross section, I the second moment of cross section, w and ψ are the transverse deflection and slope of the axis of the piezoelectric ceramic tube, respectively, Q and M are the shear force and the bending moment at the cross section of the tube, respectively.

The shear force, Q, is expressed as

$$Q = \kappa A G \left(\partial w/\partial z - \psi\right), \tag{2}$$

where κ is the shear correction coefficient, which is determined by the outer and inner radii and the Poisson ratio of the tube,[11] G is the shear modulus of the piezoelectric ceramic tube.

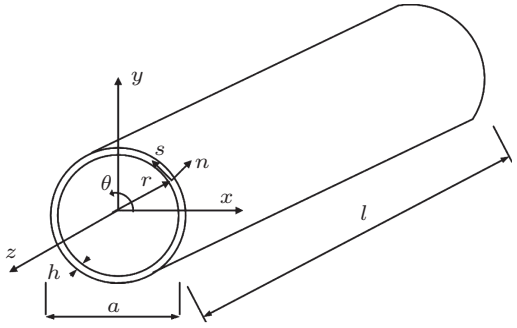


Fig. 1. Theoretical model of the tube in the scanner.

The bending moment, M, is expressed as

$$M = \int_A y \tau_z \, \mathrm{d}A, \tag{3}$$

where y is the displacement in the y direction, and τ_z is the stress component in the z direction. According to the linear constitutive equations of piezoelectricity in a local coordinate system (z, s, n), shown in Fig. 1, where the z axis coincides with the axis of the cylinder, s and n are the tangential and normal directions of the cross section, respectively, τ_z can be expressed as

$$\begin{aligned} \tau_z(n,z,t) = {} & \left[E/\left(1-\sigma^2\right)\right] \left(\varepsilon_z(n,z,t) + \varepsilon_s(n,z,t)\,\sigma \right. \\ & \left. - d_{31}(1+\sigma) E_n(n,z,t)\right). \end{aligned} \tag{4}$$

Here, $E = 1/s_{11}^E$ and $\sigma = -s_{12}^E/s_{11}^E$; s_{ij}^E (i, j = 1, 2; represent z and s directions, respectively) is the elastic constant under a constant electric field; ε_z and ε_s are the strains in the s and z directions, respectively, d_{31} is the piezoelectric strain constant, and E_n the electric field intensity in the n direction. According to the strain-mechanical displacement relations, ε_s and ε_z can be written as

$$\begin{aligned} \varepsilon_s &= \frac{1}{2}\left(\frac{\partial w(z,t)}{\partial z} - \psi(z,t)\right), \\ \varepsilon_z &= -y\frac{\partial \psi(z,t)}{\partial z}, \end{aligned} \tag{5}$$

and E_n can be expressed as[12]

$$\begin{aligned} E_n &= -\frac{v}{h} + \frac{e_{33}}{2\varepsilon_{33}^S}\frac{\partial \psi}{\partial z}\left(R_1 + R_2 - 2n\right), \\ & R_1 \le n \le R_2, \end{aligned} \tag{6}$$

where v is the electric potential difference between the outer and inner electrodes of the tube wall, h the wall thickness of the tube, e_{33} the piezoelectric constant, ε_{33}^S the dielectric constant under constant strain field, and R_1 and R_2 are the inner and outer radii of the tube. From Eqs. (3)–(6), the bending moment M can also be expressed by w and ψ.

Therefore, dynamic equation (1) of the Besocke-style scanner can be re-written as

$$\begin{cases} \kappa A G\left(\dfrac{\partial w}{\partial z} - \psi\right) - H I \dfrac{\partial^2 \psi}{\partial z^2} - \rho I \dfrac{\partial^2 \psi}{\partial t^2} = 0, \\ \rho A \dfrac{\partial^2 w}{\partial t^2} - \kappa G A\left(\dfrac{\partial^2 w}{\partial z^2} - \dfrac{\partial \psi}{\partial z}\right) = 0, \end{cases} \tag{7}$$

where $\Gamma = \left(2\sqrt{2}\left(R_1 R_2^3 - R_2 R_1^3\right) + \sqrt{2}R_1^4 - \sqrt{2}R_2^4\right)/6$, $H = \left[E/\left(1-\sigma^2\right)\right]$ for the piezoelectric tube with bipolar arrangement, and

$$H = \left[E/\left(1-\sigma^2\right)\right]\left[1 + d_{31}\frac{e_{33}}{2I\varepsilon_{33}^S}\Gamma\left(1+\sigma\right)\right]$$

for the unipolar arrangement.[13]

By defining $w(z,t) = Y\,\mathrm{e}^{\mathrm{j}\omega t}$, $\psi(z,t) = \Psi\,\mathrm{e}^{\mathrm{j}\omega t}$, $\xi = z/l$, $b^2 = \rho A l^4 \omega^2/(HI)$, $r^2 = I/Al^2$, and $s^2 = HI/\kappa A G l^2$, the harmonic solution of Eq. (7) is given as[14]

$$\begin{cases} Y = C_1\cosh(b\alpha\xi) + C_2\sinh(b\alpha\xi) \\ \qquad + C_3\cos(b\beta\xi) + C_4\sin(b\beta\xi), \\ \Psi = k_1 C_1\sinh(b\alpha\xi) + k_1 C_2\cosh(b\alpha\xi) \\ \qquad + k_2 C_3\sin(b\beta\xi) - k_2 C_4\cos(b\beta\xi), \end{cases} \tag{8}$$

$$\begin{pmatrix} \alpha \\ \beta \end{pmatrix} = \frac{1}{\sqrt{2}}\left(\mp\left(r^2+s^2\right) + \sqrt{\left(r^2-s^2\right)^2 + \frac{4}{b^2}}\right)^{1/2}, \tag{9}$$

where the coefficients C_1, C_2, C_3, C_4, and k_1, k_2 are determined by the sizes, material constants, and angular frequency of the flexural vibration of the piezoelectric tube.

3. Boundary conditions for the Besocke-style scanner

For the two kinds of Besocke-style scanners shown in Fig. 2, a static friction acting on the ball is considered during the scanner being in the scanning motion.[10] The effects of the friction between a sapphire (or steel) ball and the movable ramp disk (or static helical ramp), and the corresponding bending moments are taken into account. Therefore, the exact boundary conditions for the two Besocke-style scanners are given as follows.

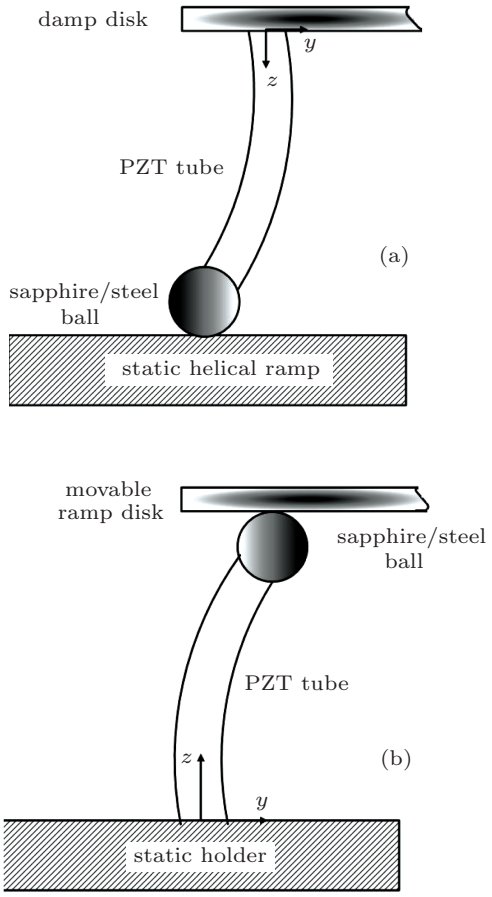


Fig. 2. Schematic diagrams of Besocke-style scanners.

3.1. Characteristic equation of flexural vibration for case A

For case A, shown in Fig. 2(a), a damp disk is soldered on one end of the piezoelectric ceramic tube, which can move following the vibration of the tube, in which the damp disk horizontally moves and the slope at the side is zero. The boundary conditions can be obtained as

$$\begin{cases} \left[\kappa AG\left(\dfrac{1}{l}\dfrac{\partial Y}{\partial \xi}-\Psi\right)+m_0\omega^2 Y\right]\Big|_{\xi=0}=0, \\ \Psi|_{\xi=0}=0. \end{cases} \tag{10}$$

Fixed at the other end of the tube is a ball which rests on a static helical ramp. According to the dynamic equilibrium for the transverse shear force and bending moment, the boundary conditions can be obtained as[9]

$$\begin{cases} \left[\kappa AG\left(\dfrac{1}{l}\dfrac{\partial Y}{\partial \xi}-\Psi\right)+f_1\omega^2\Psi-m_1\omega^2 Y\right]\Big|_{\xi=1} \\ \qquad +F/\,\mathrm{e}^{\mathrm{j}\omega t}=0, \\ \left(HI\dfrac{1}{l}\dfrac{\partial \Psi}{\partial \xi}-J_1\omega^2\Psi+f_1\omega^2 Y\right)\Big|_{\xi=1} \\ \qquad -Fd/\,\mathrm{e}^{\mathrm{j}\omega t}=0, \end{cases} \tag{11}$$

where m_0 is the mass of the damp disk, m_1 the mass of the ball, f_1 the first moment of m_1, J_1 the inertia moment of m_1, F the friction acting on the ball by the static helical ramp, and d the distance between the center of the cross section of the tube end ($\xi=1$) and the ramp. It is assumed that the protruding length of the ball into the tube is very short, and d can be approximately regarded as the diameter of the ball.

The scanner head in Fig. 2(a) is taken as an equilibrating force system during the harmonic vibration. According to the dynamic equilibrium at the flexural vibration of the tube with mass loads, the friction F can be obtained by

$$F=M+N, \tag{12}$$

where

$$M=\left(m_0\omega^2 Y\,|_{\xi=0}+m_1\omega^2 Y\,|_{\xi=1}-\rho A\omega^2\left(\frac{\partial Y}{\partial \xi}\bigg|_{\xi=1}-\frac{\partial Y}{\partial \xi}\bigg|_{\xi=0}\right)\right)\mathrm{e}^{\mathrm{j}\omega t},$$

$$N=\frac{\left(J_1\omega^2\Psi\,|_{\xi=1}-J\omega^2\left(\dfrac{\partial \Psi}{\partial \xi}\Big|_{\xi=1}-\dfrac{\partial \Psi}{\partial \xi}\Big|_{\xi=0}\right)\right)\mathrm{e}^{\mathrm{j}\omega t}}{d}.$$

Here, J is the inertia moment of the piezoelectric tube, M and N are the force induced by the transverse vibration and by the inertial moment of the scanner head, respectively.

Substitutions of Eqs. (8) and (12) into Eqs. (10) and (11) yield four linear equations of C_1, C_2, C_3, and C_4 as

$$[\boldsymbol{U}]\boldsymbol{C} = \boldsymbol{0}, \tag{13}$$

where $\boldsymbol{C} = [C_1,\ C_2,\ C_3,\ C_4)]$, $[\boldsymbol{U}]$ is a 4×4 matrix and $U_{11} = \mu_0 b^2 s^2$, $U_{12} = b\alpha + \eta_0 l k_1 b^2 s^2 - l k_1$, $U_{13} = \mu_0 b^2 s^2$, $U_{14} = b\beta - \eta_0 l k_2 b^2 s^2 + l k_2$, $U_{21} = k_1 b\alpha + \eta_0 b^2/l$, $U_{22} = \vartheta_0 b^2 k_1$, $U_{23} = k_2 b\beta + \eta_0 b^2/l$, $U_{24} = -\vartheta_0 b^2 k_2$, $U_{31} = \Phi\sinh(b\alpha) + \Lambda\cosh(b\alpha) + \Pi_{C_1}$, $U_{32} = \Phi\cosh(b\alpha) + \Lambda\sinh(b\alpha) + \Pi_{C_2}$, $U_{33} = -\Theta\sin(b\beta) + \Lambda\cos(b\beta) + \Pi_{C_3}$, $U_{34} = \Theta\cos(b\beta) + \Lambda\sin(b\beta) + \Pi_{C_4}$, $U_{41} = \Omega\cosh(b\alpha) + \Xi_1\sinh(b\alpha) - \Delta_{C_1}$, $U_{42} = \Omega\sinh(b\alpha) + \Xi_1\cosh(b\alpha) - \Delta_{C_2}$, $U_{43} = \Gamma\cos(b\beta) + \Xi_2\sin(b\beta) - \Delta_{C_3}$, $U_{44} = \Gamma\sin(b\beta) - \Xi_2\cos(b\beta) - \Delta_{C4}$, $\Phi = b\alpha + \eta_1 k_1 l b^2 s^2 - k_1 l$, $\Lambda = -\mu_1 b^2 s^2$, $\Pi = l\omega^2 F/KGA$, $\Theta = b\beta - \eta_1 k_2 l b^2 s^2 + k_2 l$, $\Omega = k_1 b\alpha + \eta_1 b^2/l$, $\Gamma = k_2 b\beta + \eta_1 b^2$, $\Xi_1 = -\vartheta_1 b^2 k_1$, $\Xi_2 = -\vartheta_1 b^2 k_2$, $\Delta = d_1 l\omega^2 F/EI$, $\mu_j = m_j/m$, $\eta_j = f_j/ml$, $\vartheta_j = J_j/ml^2$, $m = \rho Al$, $j = 0, 1$. Π_{C_i} and Δ_{C_i} $(i = 1, \ldots, 4)$ denote coefficients of C_i in Π and Δ, respectively.

If the non-zero solutions of $\boldsymbol{C}$ in Eq. (13) are available, the determinant $|\boldsymbol{U}|$ should be zero, and the exact characteristic equation of flexural vibrations of the outer piezo-tube can be obtained.

3.2. Characteristic equation of flexural vibration for case B

For case B, shown in Fig. 2(b), one end of the piezoelectric ceramic tube is soldered onto the static holder, and a ball is fixed at the other end of the tube. A ramp disk rests on the ball, which can move by the static friction. In this case, the static friction on the ball becomes

$$F = -m_2\omega^2 Y\,\mathrm{e}^{\mathrm{j}\omega t}, \tag{14}$$

where m_2 is the mass of the ramp disk.

Here, the tube can be regarded as a cantilever with mass loads; therefore, the boundary conditions at both ends of the tube can be obtained as

$$\begin{cases} Y\,|_{\xi=0} = 0, \\ \Psi\,|_{\xi=0} = 0, \\ \left[\kappa AG\left(\dfrac{1}{l}\dfrac{\partial Y}{\partial\xi} - \Psi\right) + f_1\omega^2\Psi - m_1\omega^2 Y\right]\Big|_{\xi=1} \\ \qquad + F/\,\mathrm{e}^{\mathrm{j}\omega t} = 0, \\ \left(HI\dfrac{1}{l}\dfrac{\partial\Psi}{\partial\xi} - J_1\omega^2\Psi + f_1\omega^2 Y\right)\Big|_{\xi=1} \\ \qquad - Fd/\,\mathrm{e}^{\mathrm{j}\omega t} = 0. \end{cases} \tag{15}$$

In this case, $U_{11} = 1$, $U_{12} = 0$, $U_{13} = 1$, $U_{14} = 0$, $U_{21} = 0$, $U_{22} = k_1$, $U_{23} = 0$, $U_{24} = -k_2$, the others are the same as those in the case of Fig. 1(a).

For case B, if the non-zero solutions of $\boldsymbol{C}$ are available, the determinant $|\boldsymbol{U}|$ should be zero, and then the flexural resonance frequencies of the piezoelectric ceramic tube can be easily obtained by numerical calculations.

4. Results and discussion

For comparing with the experimental results, the parameters in the calculations are cited from relevant Refs. [4] and [5]. The numerically calculated results of the fundamental flexural resonance frequencies in this work are listed in Table 1, Meanwhile, the theoretical and experimental results of the relevant references are also listed.

Table 1. Theoretical and experimental fundamental resonance frequencies.

Sample	Besocke 1 (Ref. [5]) for case A	Besocke 2 (Ref. [4]) for case B	Besocke 3 (Ref. [4]) for case B
Experimental frequency/Hz	1000	1700	9500
Calculated frequency/Hz	1800	1520	9974
Relative error by references	80%	11%	5%
Calculated frequency/Hz by this work	960	1679	9612
Relative error of this work	4%	1%	1.1%

From Table 1, it is clearly shown that the calculated results using our theory are in excellent agreement with the experimental measurements. Especially for Besocke 1 in case A, the calculated result obtained by this work has much higher accuracy (the relative error 4%), but the results calculated by the other model even have a relative error of about 80%.

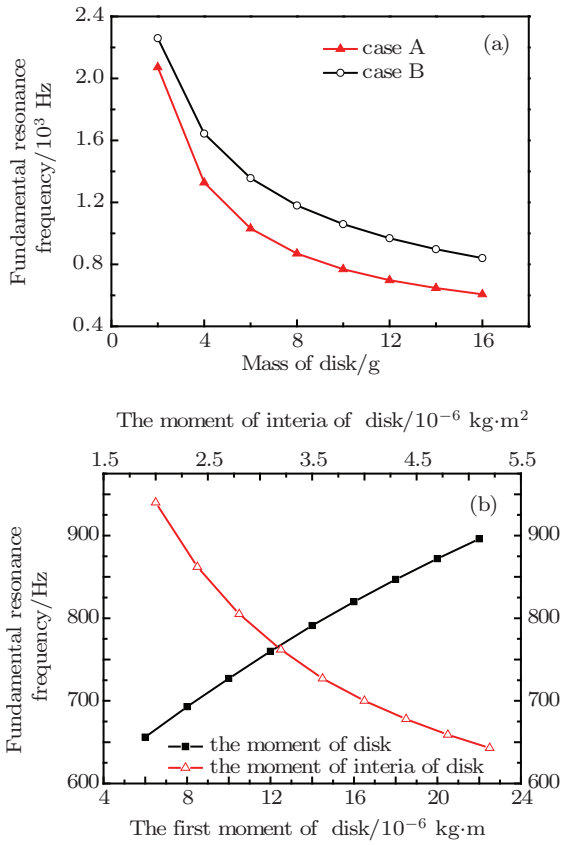


Fig. 3. (colour online) Dependences of fundamental flexural resonance frequencies with (a) mass of disk, and (b) first moment and inertia moment of disk.

In addition, the disk effect on the fundamental flexural resonance frequency is also calculated as shown in Fig. 3, in which the parameters are cited from Ref. [5] for Fig. 3(a), but for Fig. 3(b) the disk mass is chosen to be 10 g. From Fig. 3, it can be seen that for cases A and B, the fundamental flexural resonance frequency decreases with the disk mass increasing; and, for case A, the fundamental flexural resonance frequency depends also on the bending moment and rotary inertia of the disk.

Meanwhile, the effect of the bending moment induced by the friction on the flexural resonance frequency is also calculated by the presented theory as shown in Fig. 4, in which the disk mass is selected to be 10 g for Fig. 4(a), the ball mass is selected to be 0.09 g for Fig. 4(b), and other parameters in the calculations are cited from Ref. [5].

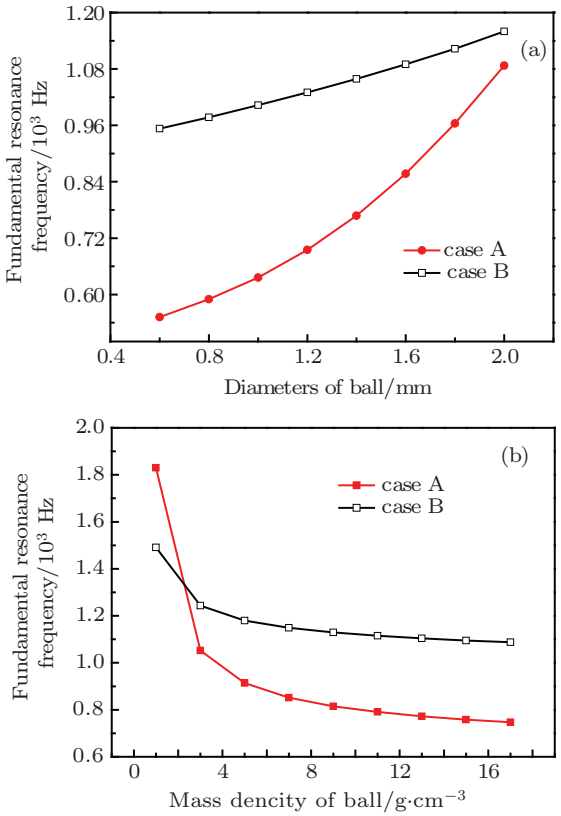


Fig. 4. (colour online) Dependences of fundamental flexural resonance frequencies on (a) diameter of ball, and (b) mass density of ball.

From Fig. 4, it can be seen that the fundamental flexural resonance frequency increases rapidly with the increase of ball diameter. Therefore, if the mass of the ball is kept constant, choosing a ball with light density can also increase the resonance frequencies. For example, in case A from Ref. [5], for a Besocke-style scanner with a sapphire ball instead of a steel ball, the fundamental flexural resonance frequency can increase by about 12% if the other parameters are unvaried.

5. Conclusion

In this paper, using the presented theory the main factors affecting the flexural resonance frequencies of Besocke-style scanners are calculated and analysed in detail. The calculated results are shown to be in excellent agreement with the measured results. In addition, the theory provides an effective method to optimize the performances of the scanners, such as how to increase the resonance frequencies of the scanners. It

is shown that in the design of the scanner structure, considerable attention should be paid to not only the parameters of the tube and disk, but also the parameters of the balls and the frictions acting on the balls. Furthermore, the theory can also be used to estimate the behaviours of ultrasonic actuators and sensors operated in a higher flexural resonance mode.

References

[1] Meyer G 1996 *Rev. Sci. Instrum.* **67** 2960

[2] Ross J P, Cai X, Chiu J F, Yang J and Wu J R 2002 *J. Acoust. Soc. Am.* **111** 1161

[3] Pertaya N, Braun K F and Rieder K H 2004 *Rev. Sci. Instrum.* **75** 2608

[4] Hua B C, Qian J Q, Wang X and Yao J E 2011 *Acta Phys. Sin.* **60** 040702 (in Chinese)

[5] Arnalds U B, Bjarnason E H, Jonsson K and Olafsson S 2006 *Appl. Surf. Sci.* **252** 5485

[6] Brukman M J and Carpick R W 2006 *Rev. Sci. Instrum.* **77** 033706

[7] Ball S J, Contant G E and McLean A B 2004 *Rev. Sci. Instrum.* **75** 5293

[8] White M W D and Heppler G R1995 *ASME J. Appl. Mech.* **62** 193

[9] Liu Y Z 2009 *Chin. Phys.* B **18** 1674

[10] Zhang H, Zhang S Y, Chen Z J and Fan L 2010 *IEEE Trans. Ultrason., Ferroelect., Freq. Control* **57** 1140

[11] Hutchinson J R 2001 *J. Appl. Mech.* **68** 87

[12] Krommer M and Irschik H 2002 *Acta Mech.* **154** 141

[13] Zhang H, Zhang S Y and Wang T H 2007 *Ultrasonics* **47** 82

[14] Rossit C A and Laura P A A 2001 *J. Acoust. Soc. Am.* **110** 2837